Electron Transfer of Hydrated Transition Metal Ions and the Electronic State of Co3+(aq)

Nielsen, Mathias T; Moltved, Klaus A.; Kepp, Kasper Planeta

Published in:
Inorganic Chemistry

Link to article, DOI:
10.1021/acs.inorgchem.8b01011

Publication date:
2018

Document Version
Peer reviewed version

Electron Transfer of Hydrated Transition Metal Ions and the Electronic State of Co3+(aq)

Journal:	*Inorganic Chemistry*
Manuscript ID	ic-2018-010116.R1
Manuscript Type:	Article
Date Submitted by the Author:	n/a
Complete List of Authors:	Nielsen, Mathias; Technical University of Denmark, DTU Chemistry Moltved, Klaus; Technical University of Denmark, DTU Chemistry Kepp, Kasper; Technical University of Denmark, DTU Chemistry

Electron Transfer of Hydrated Transition Metal Ions and the Electronic State of $Co^{3+}(aq)$

Mathias T. Nielsen, Klaus A. Moltved, and Kasper P. Kepp*

Technical University of Denmark, DTU Chemistry, Building 206, 2800 Kgs. Lyngby, DK – Denmark. *Phone: +045 45 25 24 09. E-mail: kpj@kemi.dtu.dk

Abstract.

Electron transfer (ET) is broadly described by Marcus-type theories, and plays a central role in many materials and catalytic systems and in biomolecules such as cytochromes. Classic ET processes are the self-exchange reactions between hydrated transition metal ions such as $Fe^{2+}(aq) + Fe^{3+}(aq) \rightarrow Fe^{3+}(aq) + Fe^{2+}(aq)$. A well-known anomaly of Marcus theory is Co^{2+}/Co^{3+} exchange, which proceeds ~10^5 times faster than predicted. $Co^{3+}(aq)$ is a complex and reactive system widely thought to feature low-spin Co^{3+}. We studied the self-exchange process systematically for Cr^{2+}/Cr^{3+}, V^{2+}/V^{3+}, Fe^{2+}/Fe^{3+}, Co^{2+}/Co^{3+} using six distinct density functionals. We identify directly the ~10^5 anomaly of Co^{2+}/Co^{3+} from the electronic reorganization energies without use of empirical cross relations. Furthermore, when modeling Co^{3+} as high-spin, the anomaly disappears, bringing all four processes on a linear trend within the uncertainty of experiment and theory. We studied both the acid-independent $[Co(H_2O)_6]^{3+}$ species that dominates at low pH, and the acid-dependent $[Co(OH)(H_2O)_5]^{2+}$ species that becomes important at higher pH, and use two distinct explicit second-sphere hydration models and models of perchlorate anion association. The high-spin state with weaker Co-O bonds is stabilized by vibrational energy and entropy by ~11 and ~12 kJ/mol, correcting gap estimates from absorption spectroscopy. High-spin $Co^{3+}(aq)$ explains the full experimental data series of the M(aq)

systems. Low-spin Co^{3+} and high-spin Co^{2+} involves changes in e_g occupation upon electron transfer, with associated M-O bond changes and increased reorganization energy. In contrast, with high-spin Co^{3+}(aq) the redox-active electrons shuffle between t_{2g} orbitals to minimize structural changes, producing a relative rate in excellent agreement with experiment. This e_g occupation effect explains most of the experimental differences in rate constants, with the remaining part explained by second-sphere hydration and anion effects. Our results consistently suggest that some high-spin Co^{3+}(aq) is active during the experiments.

Keywords: Electron transfer, DFT, reorganization energy, Marcus theory, metal complexes, cobalt

Introduction.

Electron transfer is the most fundamental process of chemistry and plays a central role in broad areas of catalysis and materials science and in the two fundamental life processes respiration and photosynthesis; these processes are broadly described by the semi-classical theory inspired by Libby[1] and developed by Marcus and others[2–7]. A central equation of this theory is the relationship between the reorganization energy and the overall rate of electron transfer[2], simplified as:

$$k_{ET} = A\, exp\left[\frac{-(E^0+\lambda)^2}{4\lambda RT}\right] \quad (1)$$

where E^0 is the redox potential of the reaction and λ is the reorganization energy. The pre-exponential factor A includes all the electronic and vibrational coupling of the donor and acceptor states and the normal terms describing the diffusion-controlled collision of reactants. Another central equation is the Marcus cross relation that predicts the rate of an ET process from the constituent self-exchange rates of each redox couple[2,8]:

$$k_{12} = \sqrt{k_{11}k_{22}K_{12}f_{12}} \quad (2)$$

where k_{12} is the cross ET between two different systems, K_{12}, is the equilibrium constant of the cross reaction, k_{11} and k_{22} are the corresponding self-exchange rate constants for each system, and f_{12} relates the other terms to the total pre-exponential factor[2,9]. Marcus theory has commonly been tested by exploring the validity of equation (2).

A particularly classic electron transfer process is the self-exchange between hydrated transition metal ions such as $Fe^{2+}(aq) + Fe^{3+}(aq) \rightarrow Fe^{3+}(aq) + Fe^{2+}(aq)$ that figure already in the early work by Libby[1] and have implications for many electrocatalytic processes[2,9–11]. These self-exchange reactions challenge the theory by apparently not all following the "pure" outer-sphere

mechanism: A particular well-known anomaly is the self-exchange of the Co^{2+}/Co^{3+} pair (k_{ET} ~5 $M^{-1}s^{-1}$)[12], which is much faster than predicted[13] from equation (2) using Marcus theory[2]. Two explanations have been given for this anomaly, one by Winkler *et al*.[14] involving a high-spin state rather than the commonly assumed and observed low-spin state of hydrated Co^{3+}, a hypothesis also discussed by Sutin[15], and the other involving a deviation from the outer-sphere mechanism by ligand bridging between the two cobalt centers as suggested by Endicott *et al*.[13]

The question of the spin state of hydrated Co^{3+} is of substantial interest on its own: Water being a relatively weak-field ligand induces high-spin in all other hexaqua ions of the first row of the d-block, yet the +3 charge and maximal ligand field stabilization energy of the t_{2g}^6 configuration causes Co^{3+} to have the largest low-spin propensity among these systems[16]. Fe^{2+} also has maximal ligand field stabilization energy in low-spin but only +2 charge and thus has larger propensity to be high-spin than Co^{3+}.[16] The opposed effects of the metal ion and ligand bring Co^{3+}(aq) conspicuously close to spin crossover (SCO), as argued already by Taube *et al*.[17], and evident from comparison of metal-ligand combinations using spin-state-balanced density functional theory (DFT)[16]. In fact, since $[CoF_6]^{3-}$ is high-spin and $[Co(H_2O)_6]^{3+}$ is broadly thought to be low-spin, there is some ligand field strength between F^- and H_2O in the spectrochemical series that produces SCO for Co^{3+}; these two ligands are close in the series indicating by itself that high-spin is not very high in energy in Co^{3+}(aq).

Taube *et al*. found low-spin Co^{3+}(aq) in their magnetic measurements[17]. Absorption spectroscopy puts the high-spin state ~0-37 kJ/mol above low-spin[14], whereas NMR paramagnetic shifts were used by Navon to suggest > 23 kJ/mol[18]. Taube and co-workers[17] and Winkler, Rice, and Gray[14] suggested high-spin to be at +17 kJ/mol once correcting the vertical excitation data by Johnson and Sharpe[19] for the high-spin excited state geometric relaxation.

These reports have been used to argue against a high-spin mechanism of self-exchange ET[10]. A cobalt cluster was synthesized with a fixed coordination-number, preventing inner-sphere reaction, and a presumably higher propensity to be high-spin than Co^{3+}(aq) *viz*. its oxygen-donor ligand field; this cluster still displayed low-spin Co^{3+} and a slow exchange rate, in support of an inner-sphere mechanism of Co^{3+}(aq) as it is then apparently not high-spin[10]. The interpretation has implications for the rationalization of other processes, *e.g.* the self-repair function of cobalt-based oxygen-evolving complexes, which relies on fast cobalt electron transfer[10].

A major problem in all experimental reports on Co^{3+}(aq) is its complexity and reactivity in solution: The solution may contain dimeric species and standard protocols invoke strong acid to study the system[20], and only a few crystal structures have been obtained that include the hexaquacobalt(III) first coordination sphere[21]. Thus, the interest is not in a complete account of all species present under various conditions, but an account of the species that must be chemically active to explain the experimental data.

In this work, we obtain directly from DFT-derived electronic reorganization energies the Co^{2+}/Co^{3+} anomaly of Marcus theory. Using equation (1) and because E^0 for these self-exchange processes is zero, if these are all outer-sphere reactions we expect a linear fit of the type:

$$ln\, k_{ET} = \frac{-\lambda}{4RT} + lnA \qquad (3)$$

Thus, if Marcus outer-sphere theory is valid and the reactions otherwise behave similarly, we should have the strong linear requirement:

$$ln\, k_{ET} \propto -\lambda \qquad (4)$$

If the experimental data correlate with electronic reorganization energies, outer-sphere Marcus theory is valid for the systems and process observed. Any deviation from a straight line on the other hand indicates that the systems of interest are not explained by Marcus theory, or the errors in the computed or experimental data are too large to show such a linear relationship.

We discuss the involvement and accessibility of the high-spin state of Co^{3+}(aq), and we reinterpret previous reports[14,17,18,22]. It is well-known that vibrational zero-point and entropy differences both favor the more loosely bonded (due to occupation of the e_g orbitals) high-spin states of mononuclear coordination complexes by 10−15 and 10−30 kJ/mol, respectively[23–25].

The M^{3+}(aq) complexes have $pK_a \sim 2-4$[26,27] and are thus deprotonated in their first hydration sphere unless in strong acid. The Brønsted acidity[26] affects the electronic structure and self-exchange by producing two contributions to the overall observed rate; one due to the protonated species (k_1) that dominates completely at low pH, and one due to the deprotonated species that builds up at higher pH (k_2)[12]:

$$rate = k_{ET}[Co(II)][Co(III)] = \left[k_1 + \frac{k_2}{[H^+]}\right][Co(II)][Co(III)] \quad (5)$$

We show below that the cobalt anomaly disappears to within the uncertainty in experimental and theoretical methods with high-spin Co^{3+}(aq); the result is robust against structural model, choice of experimental data, and theoretical method. The rate differences are almost completely described by structural changes caused by e_g orbital occupation. We argue that the anomaly has arisen from use of rate constants in cross reactions based on low-spin Co^{3+}, which produce slower ET with reduced redox partners that have e_g partially occupied, whereas high-spin Co^{3+} is fast.

Computational Methods.

We studied the hexaqua complexes and larger second-sphere hydrated models of the transition metal ions Co^{2+} and Co^{3+} and also of several related systems Cr^{2+}/Cr^{3+}, V^{2+}/V^{3+}, and Fe^{2+}/Fe^{3+}, for which experimental self-exchange rate constants have been reliably produced by several groups[9,11,28–31]. Mn^{2+}/Mn^{3+} has received less attention due to experimental issues, and results vary by 5 orders of magnitude[15], which is not reliable enough to infer any specific mechanism; thus they were not included in the lists by Chou *et al*.[28], Newton and Sutin[9], and in this work.

All computations were performed using the Turbomole software, version 7.0[32]. All densities and energies were converged to 10^{-6} a.u., and the resolution of identify approximation was used to speed up all calculations[33,34]. To enable correct computation of the reorganization energies at their exact positions on the potential energy surfaces, we computed both the energies and the fully optimized geometries using the fully polarized def2-TZVPP basis set[35], with polarization functions also on hydrogen to account for the polarization effects of the many water protons during geometry relaxation upon electron transfer.

Six density functionals were investigated to understand how such methods perform: PBE and PBE0[36] as representative non-empirical GGA and hybrid functionals, B-LYP and B3-LYP[37–39] as representative non-hybrid and hybrid functionals using the LYP correlation functional, and TPSS and TPSSh[40,41] as representative non-hybrid and hybrid meta functionals. PBE0 and B3-LYP include 25 and 20% HF exchange, whereas TPSSh includes 10% HF exchange.

The self-exchange inner-sphere reorganization energies were computed as[42]:

$$\lambda = E_{el}(M^{2+}(M^{3+})) - E_{el}(M^{2+}(M^{2+})) + E_{el}(M^{3+}(M^{2+})) - E_{el}(M^{3+}(M^{3+})) \quad (6)$$

where $E_{el}(M^{2+}(M^{3+}))$ is the electronic energy evaluated as the converged single-point energy of species M^{2+} on the optimized geometry of species M^{3+}. To ensure accurate reorganization

energies, all energies were computed using the exact same method and basis set for all six functionals, *i.e*. the geometries of all models were optimized separately using all six functionals. All the optimized structures are in supplementary xyz-files and the electronic energies are reported for easy reproducibility in the Supporting Information, **Tables S1−S24**.

To account for solvation effects the dielectric continuum model COSMO was used consistently for both geometry optimizations and single-point energies[43,44]. The electrostatic screening improves the vertical ionization energies and electron affinities used to compute λ[45,46]. To describe the electrostatic screening of water, $\varepsilon = 80$ was used for all computations. As the effective radius of solvation, the default optimized radii were used for all atoms, except for the metal ions which were modeled using a radius of 2.0 Å, as usually applied[23] (this has little effect on coordination-saturated complexes but may affect unsaturated complexes where the solvent probe approaches the metal ion[47–49]. Varying the radius from 1.4−2.7 Å changed Cosmo solvation energies by maximally ~6 kJ/mol[48]).

Long range dispersion interactions were accounted for using the D3 dispersion correction[50], applied to all calculations, both geometry optimizations and single-point energies, because the reorganization energies in principle require the energies to be evaluated at the exact minima of the potential energy surfaces, *i.e*. obtained using the same method. We know from previous work[16] that the dispersion forces favor the more compact M^{3+} states and in the case of the Co^{3+}, the low-spin state more than the high-spin state, and these dispersion effects are non-negligible.

The effect of spin state was investigated by performing geometry optimization of Co^{2+}(aq) and Co^{3+}(aq) in both spin states. **Tables S25-S27** provide numerical information on the gap between high-spin and low-spin. Co^{2+}(aq) was only studied for comparative purposes at it is

clearly high-spin. The geometry-optimized Co^{3+}(aq) structures in both spin states were used to compute the reorganization energy as in the other M(aq) systems.

Because the pK_a values of the M^{3+}(aq) complexes vary between 2−4[51,52], two species are relevant, one acid-independent species $[M(H_2O)_6]^{3+}$ that controls k_1, and one $M(H_2O)_5OH]^{2+}$ that controls k_2 of Equation (5); the importance of the latter increases with pH. We thus also investigated models with a deprotonated water in the first hydration sphere. Models with a second hydration sphere were also consistently studied for all complexes such that the compensating second-sphere hydrogen bonding effects on structural reorganization were accounted for. To estimate the absolute potentials, the electronic energies of the deprotonated M^{3+} systems were reported with the proton affinity of water added, *i.e.* $E_{H_3O^+} - E_{H_2O}$, calculated following the same procedure as other molecules (see Supporting information, **Table S29**). Standard half potentials $E_{½}^{0}$ were computed from the fully geometry-relaxed ground states by correcting for the absolute potentials of the hydrogen electrode (4.42 V). As we study relative potentials and reorganization energies, these terms cancel out and thus have no influence on the reported trends that form the basis of our conclusions.

The rates of self-exchange have been measured by several groups, and thus we validate our conclusions against the sensitivity to the experimental variability. The experimental rate constants are compiled in **Table S30**, and the effect on the linear correlations are compiled in **Tables S31-S43**. These data include the squared correlation coefficient R^2, the slope, and intercept of the linear regression plots of experimental vs. calculated reorganization energies, *viz.* equation (4).

To account for both limits of symmetric and asymmetric second-sphere hydration, two models were consistently studied that arose during the optimization: Structure A was

asymmetric, whereas structure B was spherical, both representing distinct local minima upon geometry optimization that could be obtained for all complexes to ensure consistent comparison. The final geometry optimized metal-oxygen bond lengths of all models are provided in Supporting Information, **Tables S44-S57**.

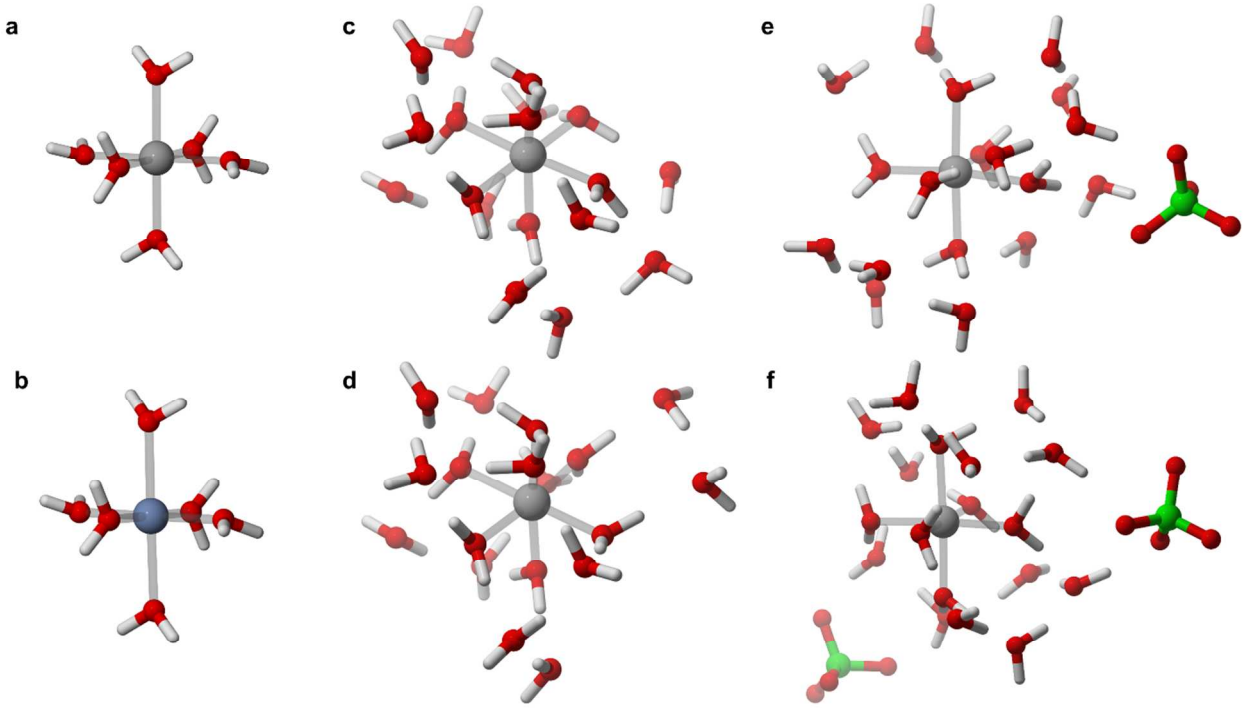

Figure 1. Examples of structural models studied in this work: **a**) $[V(H_2O)_6]^{2+}$; **b**) $[Cr(H_2O)_6]^{2+}$; **c**) Second-sphere model A (extended) of $[V(H_2O)_6]^{2+}$; **d**) Second-sphere model B (spherical) of $[V(H_2O)_6]^{2+}$; **e**) Second-sphere model B of $[V(H_2O)_6]^{3+}$ with one perchlorate; **f**) Second-sphere model A of $[V(H_2O)_6]^{3+}$ with two perchlorates.

Results and Discussion.

Equilibrium structures and self-exchange reorganization energies. The studied self-exchange processes display similar negative entropies of activation, which indicate similar behavior, (one might expect an inner-sphere reaction to have a smaller entropy of activation). Below we show that this similarity is probably not coincidental. Weaver and Yee[11] estimated the activation entropies as −15 kJ/mol for Co^{3+}/Co^{2+} and −19 kJ/mol for the other three exchange processes at 298 K; the difference of 4 kJ/mol in favor of Co^{3+}/Co^{2+} does not explain the anomaly. Most of the exponential rate dependence is therefore most likely due to variations in the inner-sphere reorganization energy where the metal-oxygen bond lengths contract upon oxidation and expand upon reduction[16]. The energy costs of these changes may be quite distinct for the four systems, and may also be affected by the second hydration shell although probably to a much smaller and similar extend, although this needs investigation. Beyond the second hydration shell, bulk water is expected to behave similarly as the same charge changes occur within the hydration spheres.

To test these assumptions, we studied models with both the first hydration sphere (**Figure 1a and 1b**) and with a second hydration sphere of 18 water molecules described by two types of geometries: An elongated asymmetric second shell structure (Geometry A, **Figure 1c**), and a more spherical second shell structure (Geometry B, **Figure 1d**). Geometry A and B represent distinct cases of asymmetric and symmetric second-sphere hydration that provide a test of the sensitivity of our results to variations in the second-shell hydration structure. This difference in second-sphere hydration does not affect the trend, nor the cobalt anomaly and its removal; however, the difference does affect the magnitude of the reorganization energies, *vide infra*. We also study both the acid-dependent and independent species, including the effect in strong acid of the perchlorate interactions with one or two anions, **Figure 1e** and **Figure 1f**. Our results show

systematic behavior due to second-shell structure, and show that the two geometries are distinct local minima that can be obtained for all systems.

The M-O bond lengths of all models have been collected for easy overview in **Tables S44-S57**. The most notable observations from the geometry optimized models are that i) all six functionals produce very similar structures for the three types of models; ii) the Jahn-Teller distorted d^4 configuration is very pronounced in Cr^{2+}(aq) in all three models; the other metal ions are generally symmetric. The tetragonal distortion of Cr^{2+}(aq) is seen in **Figure 1b** compared to the corresponding vanadium(II)complex in **Figure 1a**. The water ligands in the hexaqua models are not very bent indicating that the repulsion of the hydrogens partly compensates the tetrahedral requirements of the water lone pairs. In the large models (**Figures 1c-1f**), the water ligands bend to accommodate the hydrogen bond requirements of second-sphere water molecules; this is the most important structural effect of second-shell hydration.

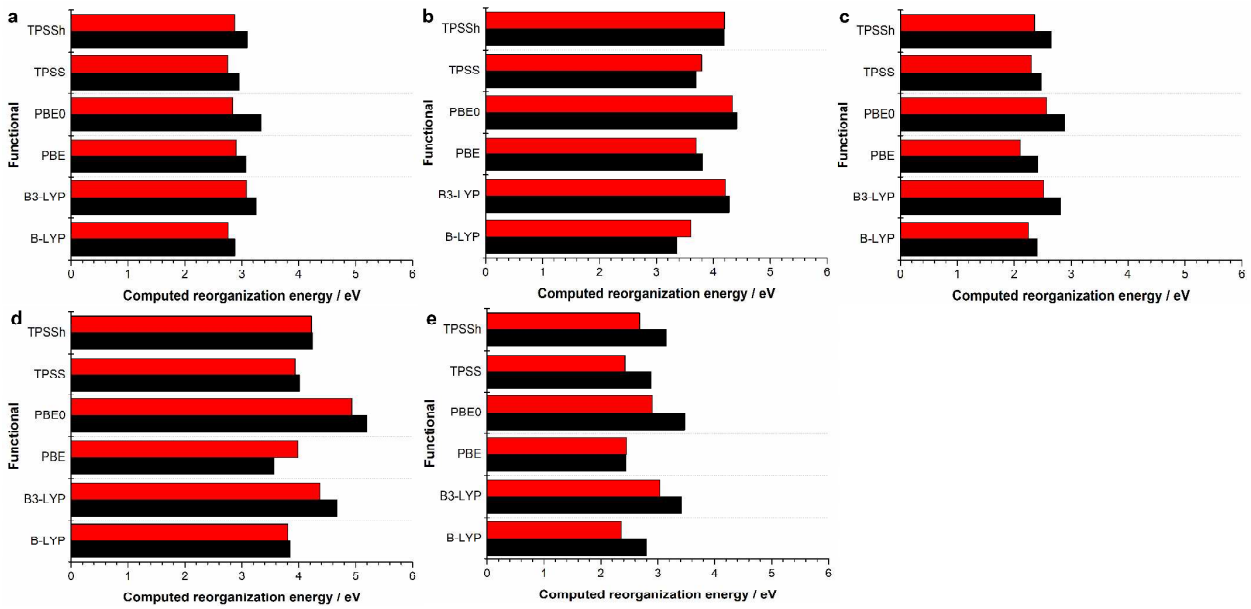

Figure 2. Sensitivity of computed reorganization energies (λ) to changes in the second hydration sphere represented by Geometry A (black) and Geometry B (red) models. **a**) the weakly distorted (in the trivalent state) V^{2+}/V^{3+} redox pair; **b**) the strongly Jahn-Teller distorted (in the divalent state) Cr^{2+}/Cr^{3+} redox pair; **c**) the weakly distorted (in both oxidation states) Co^{2+}/Co^{3+} high-spin redox pair; **d**) the Co^{2+}/Co^{3+} redox pair with low-spin Co^{3+}; **e**) the weakly distorted Fe^{2+}/Fe^{3+} redox pair.

The computed reorganization energies for all the second-shell systems in **Figure 2** reveal substantial differences of the order of 1−2 eV in λ. The total magnitudes are similar to the experimental estimates by Delahay and Dziedzic in the range 2-4 eV[53]. Second, the two types of hydration spheres produce distinct reorganization, with the elongated asymmetric second-shell hydration structure, Geometry A (black) producing larger λ than the spherical second-shell hydration structure, Geometry B (red) by up to 0.5 eV. Geometry B has more direct hydrogen bond interactions that dampen the water reorientation. This observation is fairly general (3 exceptions out of 30 comparisons) across all studied systems and density functionals. Third and

more importantly, the differences in λ can be directly explained from the changes in d-electron configuration of the involved metal ions: Thus, the Co^{3+}/Co^{2+} redox pair with Co^{3+} in the dominating low-spin state behaves similar to the strongly Jahn-Teller distorted (in the Cr^{2+} state) Cr^{3+}/Cr^{2+} self-exchange process, with all reorganization energies > 3.4 eV (3.4−5.2 eV). In contrast, a hypothetical high-spin-high-spin Co^{3+}/Co^{2+} redox pair behaves very similarly to the *other* weakly distorted systems V^{3+}/V^{2+} and Fe^{3+}/Fe^{2+} redox pairs (all reorganization energies < 3.4 eV, 2.4−3.4 eV). This observation turns out to be important, because it implies that *low-spin* Co^{3+} *will produce rates of self-exchange similar to that of the* Cr^{3+}/Cr^{2+} *pair if the processes are outer-sphere reactions.* This is, interestingly, similar to the five order of magnitude anomaly of the Co^{3+}/Co^{2+} system[10], with experimental rates of Cr^{3+}/Cr^{2+} and Co^{3+}/Co^{2+} of 10^{-5} and 5 $M^{-1}s^{-1}$.

The large reorganization energies are consistently seen when the process changes the e_g occupation, causing a major structural reorganization of the M-O bonds, which specifically happens for Cr^{3+}/Cr^{2+} and for Co^{3+}/Co^{2+} if Co^{3+} is low-spin, but *not* if it is high-spin. In contrast, the redox-active electrons of the V^{3+}/V^{2+} and Fe^{3+}/Fe^{2+} pairs shuffle between t_{2g} orbitals which exert little effect on the M-O bond lengths and thus on the structural rearrangement and λ.

Reorganization energies of low-spin Co^{3+}(aq) reproduce the cobalt anomaly. Some heterogeneity is seen in the data reported in the literature, exemplified by the compilations of Chou *et al*. and Weaver and Yee[11,28] (Supporting Information, **Table S30**). To account for this, we first studied the self-exchange rate constants compiled by Chou *et al*.[28] but then investigated the sensitivity of the correlations to the choice of other experimental estimates (**Tables S31-S37**). The experimental data shown in the figures below are thus $\ln k_{ET}(Fe^{3+}/Fe^{2+}) = 1.39$, $\ln k_{ET}(Co^{3+}/Co^{2+}) = 1.61$, $\ln k_{ET}(Cr^{3+}/Cr^{2+}) = -11.51$, and $\ln k_{ET}(V^{3+}/V^{2+}) = -3.91$[28]. The variation in experimentally reported $\ln k_{ET}$ is largest for V^{3+}/V^{2+} (~2), whereas other variations are

substantially smaller. Regardless of the differences, it is well established that Fe^{3+}/Fe^{2+} and Co^{3+}/Co^{2+} are of similar rate, V^{3+}/V^{2+} is substantially slower, and Cr^{3+}/Cr^{2+} is again much slower than any of these. Accordingly, the experimental errors are numerically substantially smaller than the trend range and the Co^{3+}/Co^{2+} anomaly, as seen from the discussion below and in the Supporting Information, **Tables S31−S37**.

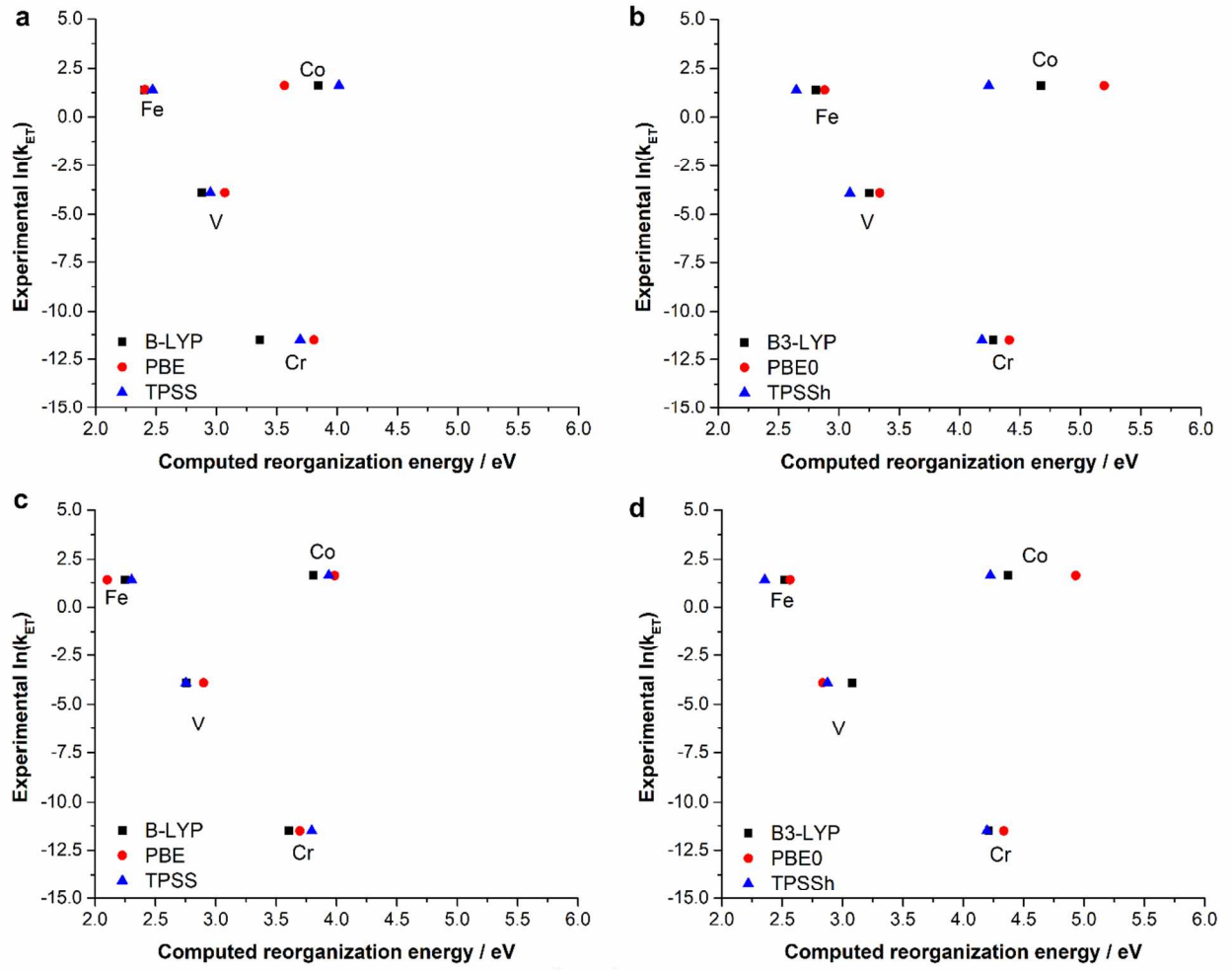

Figure 3. The experimentally measured M^{2+}/M^{3+}(aq) self-exchange rate constants vs. computed reorganization energies using low-spin Co^{3+}(aq) and the second-sphere models: **a**) non-hybrid GGA functionals and Geometry A; **b**) hybrid functionals and Geometry A; **c**) non-hybrid GGA functionals and the spherical Geometry B; **d**) hybrid functionals and Geometry B.

Figure 3 shows computed λ vs. experimental $\ln k_{ET}$ when assuming that Co^{3+} is low-spin, using the second-sphere models and divided into the three non-hybrid (**Figure 3a, 3c**) and hybrid functionals (**Figure 3b, 3d**). Cobalt is clearly an outlier from the linear trend in both plots. Regardless of the used method, this anomaly amounts to $\ln k_{ET}$ ~13, corresponding to ~$5 \cdot 10^5$, very close to the experimentally established anomaly. The computed reorganization energies of Co^{3+}/Co^{2+} and Cr^{3+}/Cr^{2+} are similar, as are their experimental rates. Thus, Co^{3+} cannot be low-spin and follow an outer-sphere mechanism at the same time, *i.e.* if the high-spin state is not accessible, a distinct mechanism needs to be invoked for Co^{3+}/Co^{2+}. These results used the $[M(H_2O)_5(OH)]^{2+}$ species, which is responsible for the acid-dependent self-exchange process that becomes more important in weaker acid and neutral pH[12]. Below, we perform a similar analysis using the more elaborate model with perchlorate anions included in the fully protonated species that govern the acid-independent pathway.

Analysis of High-Spin Co^{3+}(aq). We now explore the hypothesis that the high-spin state of Co^{3+} is active via an outer-sphere process. Water is a weak-field ligand that induces high-spin in all other hexaqua complexes of the first row of the d-block. However, the low-spin tendency of Co^{3+} is very high[16] due to its maximal ligand field stabilization energy in the t_{2g}^6 configuration and a +3 charge. According to spin state propensities computed from DFT, all halide ligands produce high-spin in Co^{3+} complexes and water produces a modest gap between the spin states[16]. $[CoF_6]^{3-}$ is known to be high-spin as the other aqua complexes. For these various reasons, Co^{3+}(aq) is an exception, and we expect the high-spin state to be close in energy. Indeed, the energy gap has been spectroscopically estimated to be ~0-37 kJ/mol with low-spin being lowest[14]; NMR studies suggest that the gap is > 23 kJ/mol[18]. Taube and co-workers[17] and Winkler, Rice, and Gray[14] suggested that the high-spin state is probably at +17 kJ/mol by

correcting the vertical excitation energy with estimates of the geometric relaxation of the high-spin state.

From comparison of the optimized energies of the low-spin and high-spin Co^{3+} states, the six functionals give energy splittings similar to the experimental estimate, with a range from -7 kJ/mol (PBE0) favoring high-spin to +57 kJ/mol (TPSS), favoring low-spin. TPSSh, which has previously been shown to predict SCO of cobalt complexes well[54], gives a value of 37 kJ/mol in favor of low-spin. The good agreement with experiment was expected, based on results from prior functional benchmarking[24,54].

The zero-point energy and vibrational entropy both favor the high-spin state with its longer and weaker metal-ligand bonds, and these effects are important to any reaction involving multiple spin states[23]. For Co^{3+}(aq), the estimated corrections are ~11.3 kJ/mol (for ZPE) and ~11.8 kJ/mol (for $T\Delta S$ at 298.15 K) both in favor of high-spin (Supporting Information, **Table S28**), based on the computed vibrational state functions of both geometry optimized spin states of the hexaquacobalt(III) complex[16]. These numbers are comfortably within the expected range of such corrections in favor of the high-spin[23,24]. Accordingly, the computed 11.8 kJ/mol entropy in favor of high-spin is also quite similar to the thermodynamic estimate given by Johnson and Nelson (~8 kJ/mol at 298 K)[22]. As pointed out, Winkler and Gray's relaxation of the electronic excitation data relies on a too small Co-O symmetric stretch (357 cm^{-1}), which, when updated brings Co^{3+}(aq) into effective SCO *even* without the entropy term included.

Johnson and Nelson also calculated[22] their own estimate of the contribution of high-spin excited state geometric relaxation using a harmonic valence force field approximation and found it to be smaller (24 kJ/mol) than even the first reported number by Winkler *et al*. (43 kJ/mol)[14]. With DFT, we can compute this geometric relaxation by subtracting the vertical excited single point energy of the high-spin on the low-spin geometry from the relaxed high-spin energy; we

obtain a value of 104 kJ/mol for TPSSh-D3 (102 kJ/mol for B3-LYP* which is also known to be accurate for spin state gaps)[24]; much larger than previously estimated from valence force field considerations[22]. Because this energy is subject to high-spin low-spin error cancellation the number is more accurate than spin gaps and in this case within 2 kJ/mol with two different functionals. This relaxation energy should be subtracted from the vertical excitation energy of Johnson and Sharpe (60−85 kJ/mol) to estimate the real energy difference of the two states, which then also from this consideration comes close to SCO.

The Brønsted acidity of the $M^{3+}(aq)$ complexes with pK_a values from 2-4 also contribute to the acid-dependent process.[12] We estimate that the deprotonation increases high-spin propensity by 21−23 kJ/mol (based on comparison of the computed high-spin low-spin gaps with and without deprotonation in Geometry A, PBE0-D3 and TPSSh-D3 methods, Supporting Information). This number is insensitive to the employed method (2 kJ/mol). It follows the spectrochemical series where OH^- is a weaker ligand than H_2O. Thus, the deprotonated species $[Co(OH)(H_2O)_5]^{2+}$ that controls the acid-dependent path (k_2) has larger tendency towards high-spin than the $[Co(H_2O)_6]^{3+}$ species that contributes to the acid-independent path (k_1). The total driving force in favor of high-spin $[Co(OH)(H_2O)_5]^{2+}$ is ~33−35 kJ/mol. This correction ignores the differential zero-point energies that also favor high-spin (our estimate: 11 kJ/mol). This brings $Co^{3+}(aq)$ into the SCO regime, once the energies from spectroscopy are properly corrected.

The NMR relaxation data in strong acid were used to argue that high-spin is at +23 kJ/mol[18]; however this is very similar to the energy estimate from spectroscopy and both cannot be true, since one reflects energy and the other free energy. Indeed, the NMR data show anomalous relaxation behavior that could also, as mentioned by Navon, be explained by high-spin involvement, or by $[Co(OH)(H_2O)_5]^{2+}$; the ruling out of high-spin primarily relied on the

assumption that the low-spin to high-spin conversion is much faster than the paramagnetic relaxation rate; the basis of this calculation is not clear but it was estimated using data for iron and chromium and gave a very large rate of 10^{10} s^{-1}; even with this uncertainty, the NMR data did show very anomalous curvature compared to the straight lines obtained for the relaxation rates of definite low-spin cobalt complexes[18].

High-Spin Co^{3+} Removes the Experimental Anomaly. Figure 4 shows the experimental $\ln k_{ET}$ plotted against the computed λ when using the high-spin state of $Co^{3+}(aq)$ for the acid-dependent process, $[Co(H_2O)_5OH]^{2+}$. The plots become very linear now and the cobalt anomaly almost disappears. The linearity shows that almost all the differential reorganization effects arise from the first coordination sphere, whereas the contribution from longer range is similar for all +3 ions and for all +2 ions, such that these reorganization energies explain ~90% of the variation in experimental rate constants. The cobalt anomaly is reduced by approximately 90% when using the high-spin state.

The relevant data of Equation (3) are collected in the Supporting information, **Tables S31−S37**. Assuming low-spin Co^{3+} gives very divergent results that are not easily interpreted (**Table S31**). The average intercept with Co^{3+} in high-spin (**Table S32**) is ~ $6.5 \cdot 10^{10}$ $M^{-1}s^{-1}$ ($2.2 \cdot 10^{12}$ $M^{-1}s^{-1}$ for Geometry A and $1.9 \cdot 10^{9}$ $M^{-1}s^{-1}$ for Geometry B), which is close to the expected diffusion limit[55]. The average value of the slope for Geometry A with Co^{3+} in high-spin gives a value of −9.2 +/−1.9, which corresponds well to the theoretically expected value $(4RT)^{-1}$ ~ 9.7 eV^{-1}. Because the outer-sphere contribution is constant as seen from the linear relationship, the crossing point with the vertical axis is $\ln A - \lambda_o/4RT$. A value of 0.1 is reasonable for the latter contribution, corresponding to an outer reorganization energy of ~1 eV, and thus it does not significantly affect the preexponential factor[56].

The resolution of the cobalt anomaly partially occurs for systems having only the first hydration sphere (**Figure S1**) but becomes more complete when second hydration is included. Thus, the conclusions of this work are robust against the type of the hydration model, which also relates to the constancy of the bulk contributions. The reorganization energies are uniformly larger when using the hybrid functionals but the range remains the same, about 1.5 eV from the fastest (iron) complex to the slowest (chromium) complex. It is also notable that the strong Jahn-Teller effect of Cr^{2+}, which is fully accounted for by the DFT computations, does not cause a deviation from the linear trend: The real rate of the electron transfer processes is thus dominated by the direct effect of the change in e_g orbital occupation on the M-O bond lengths.

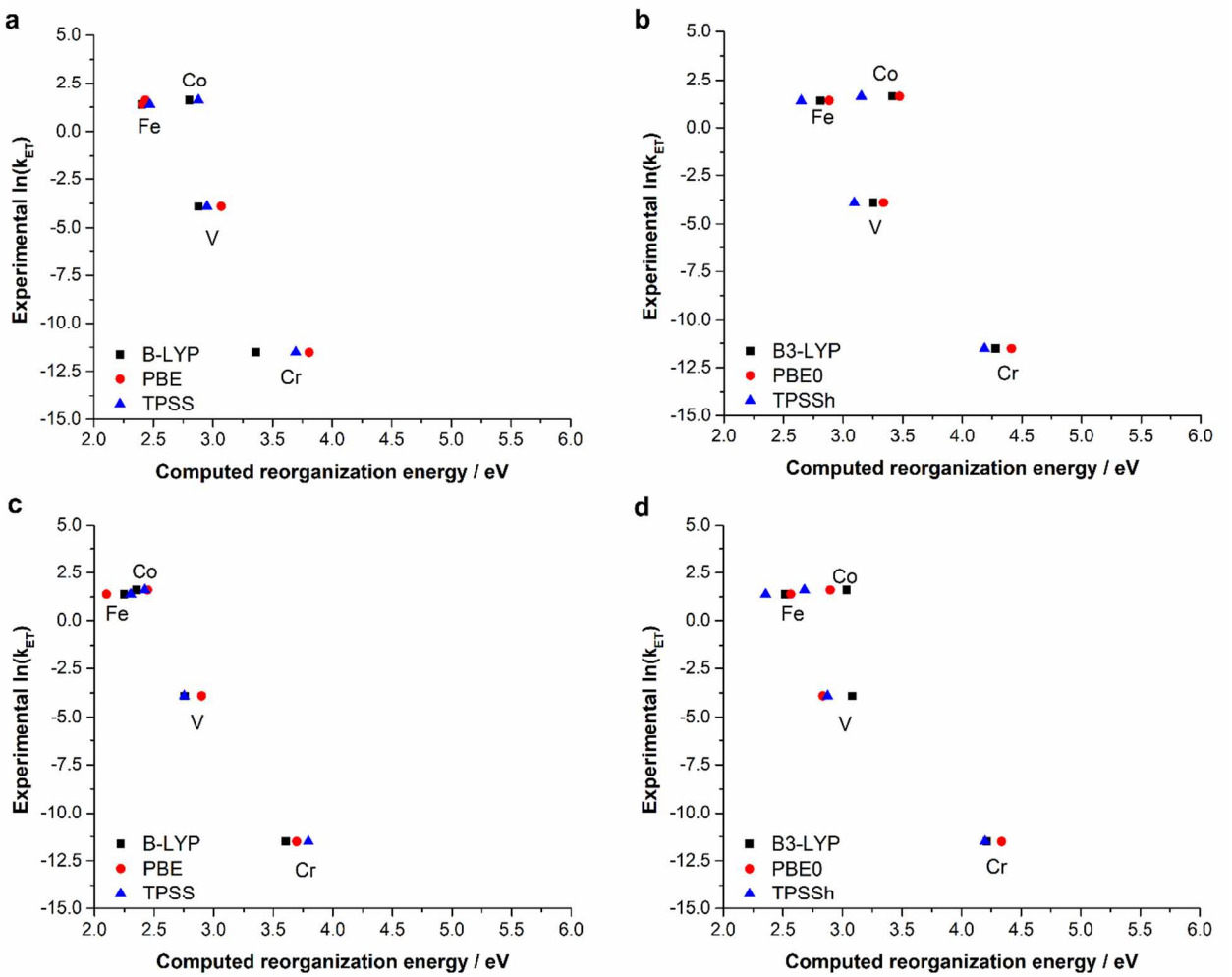

Figure 4. Same as in Figure 4, but using reorganization energies for cobalt complexes on the high-spin surface: **a**) non-hybrid GGA functionals and Geometry A; **b**) hybrid functionals and Geometry A; **c**) non-hybrid GGA functionals and Geometry B; **d**) hybrid functionals and Geometry B.

To make sure that the electronic energy calculations are fully consistent in their description of the ET processes, we also computed the relative standard half potentials ($E_{½}^{0}$, in V) from the obtained equilibrium states of the M^{3+}(aq) and M^{2+}(aq) systems, after correcting for the absolute potential of the hydrogen electrode at standard conditions (4.42 V – this term does not affect the trend). Experimental numbers used were +1.92 V for Co^{3+}/Co^{2+}, +0.77 V for

Fe^{3+}/Fe^{2+}, -0.25 V for V^{3+}/V^{2+}, and -0.41 V for Cr^{3+}/Cr^{2+}. The corresponding 12 plots of experimental vs. computed $E_{½}^{0}$ are shown in Supporting Information, **Figure S2** (six with high-spin Co^{3+} and six with low-spin). Importantly, an impaired trend is seen for the low-spin Co^{3+}(aq), whereas when we use high-spin Co^{3+}(aq), all data fall on the same line, as they should if the states are correctly described. Notice that this observation is again independent of method and strongly imply that the experimentally observed standard half potentials of the Co^{3+}/Co^{2+} redox pair are measured for high-spin Co^{3+}(aq). We also predict that the hypothetical low-spin Co^{3+}(aq), which may be measured at low to moderate temperature and strong acid, should have had a half potential that is larger (probably by 0.1-0.4 V) than the standard value +1.92 V due to the change to low-spin Co^{3+}(aq).

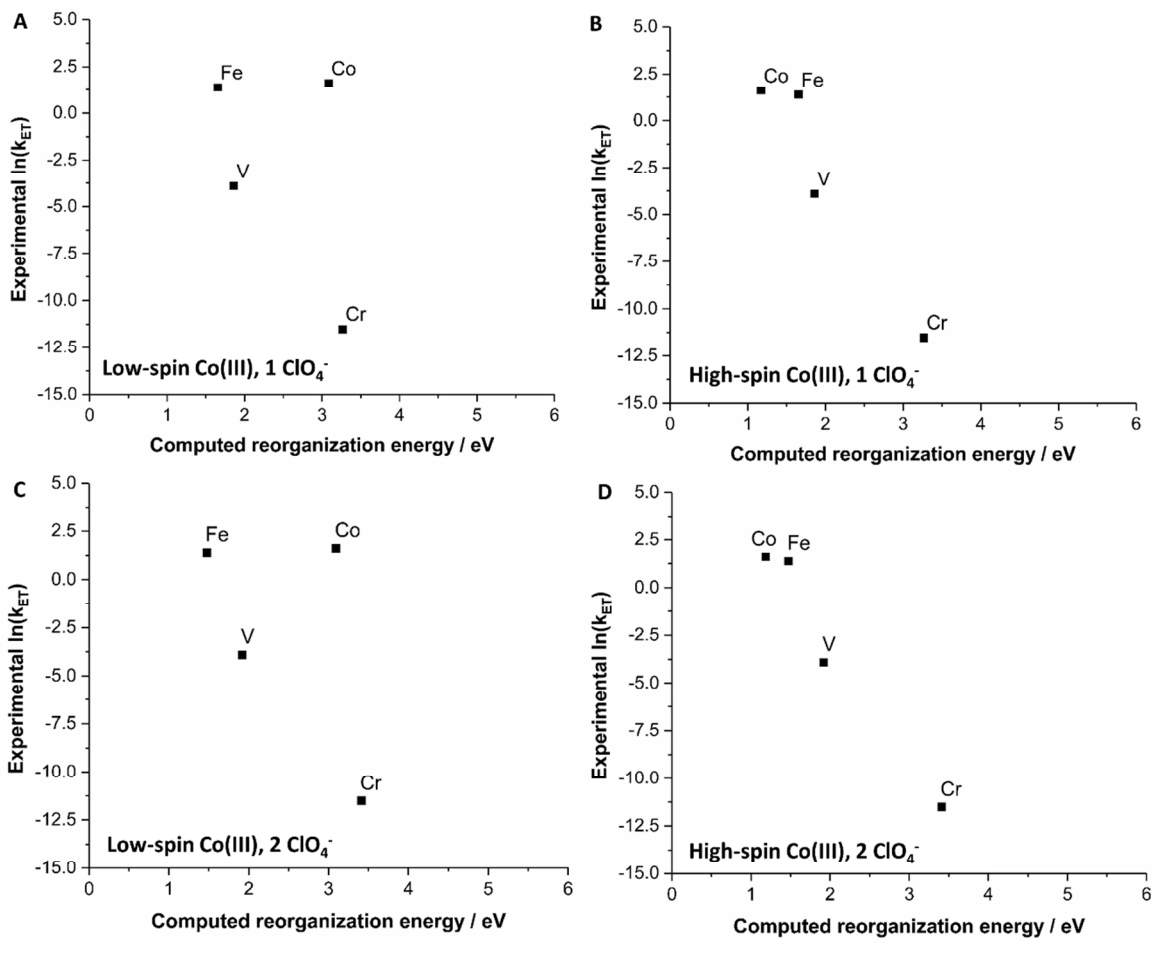

Figure 5. Plot of experimental rate constants vs. computed reorganization energies for systems with one or two perchlorate anions included in the second hydration shell as in **Figure 1e/1f** (Geometry A, PBE functional). **A**) With low-spin Co(III) and one perchlorate; **B**) with high-spin Co(III) and one perchlorate; **C**) with low-spin Co(III) and two perchlorates; **D**) with high-spin Co(III) and two perchlorates. Complete data can be found in the Supporting Information, **Tables S17-S24**.

Anion effects and the acid-dependent vs. independent processes. The experimental protocol generally involves the use of strong acid, $HClO_4$, to prevent Co(III) hydrolysis. Although it is well-known that the anions contribute little (up to 5-fold)[12] to the total rate,

consistent again with an outer-sphere mechanism where e_g occupation controls relative rates, it is of some interest to include the anion effect for completeness. **Figure 5** shows the experimental rates vs. computed reorganization energies for the large water models where one or two perchlorate anions have been added to the models in the second hydration sphere and all waters retain their protons (36 geometry optimizations, PBE functional, using both low-spin and high-spin Co(III) and both geometries A and B). **Figure 5** shows only geometry A, as geometry B gives very similar results (Supporting Information, **Tables S17-S24**). Perchlorate is known to be unlikely to form direct complexes[12] so the second-sphere association is the most prevalent perturbation that could be encountered in the real systems.

The plots in **Figure 5** show that the cobalt anomaly is still well recovered when using the strong $HClO_4$ system. In fact, the inclusion of one and in particular two anions slightly improves the correlation to make the anomaly completely disappear. Thus, the remaining 10% of the anomaly can plausibly be explained by second-sphere anion interactions. We also note that the reorganization energies for Co^{3+}/Co^{2+} are ~1 eV smaller in strong acid, indicating that the acid-independent rate constant (k_1), which is dominated by the $[Co(H_2O)_6]^{3+}$ species, is larger than the acid-independent rate constant (k_2), which is dominated by the $[Co(OH)(H_2O)_5]^{2+}$ species; this is in agreement with and explains the behavior observed by Habib and Hunt[12].

While Co^{3+}/Co^{2+}(aq) proceeds 5 orders of magnitude faster than "expected", the cluster synthesized by Ullman and Nocera to argue against high-spin Co^{3+}(aq) turned out to proceed 6 orders of magnitude *slower* than predicted from the calculations and much slower than Co^{3+}/Co^{2+}(aq). They argued that this is due to the presence of bridging inner-sphere reaction in Co^{3+}/Co^{2+}(aq) that is unavailable in the cluster, and the cluster Co^{3+} was presumed to have more high-spin propensity than Co^{3+}(aq), ruling out the spin state explanation. However, it is notable that the structure features low-spin Co^{3+}, which would almost exactly cause the slow rate

observed (as estimated from **Figure 2**). The crystal structures feature average Co-O bond lengths for the redox-active central Co^{3+} of 1.918 Å and is less paramagnetic than the Co^{2+} analogue, which has average Co-O bond lengths of 2.092 Å. DFT-BP86 calculations produce typical average errors of maximally 0.02-0.03 Å for such bond lengths (individual errors can be larger)[57]; when applied to the hexaquacobalt(III) and heaxaquacobalt(II) systems it gives average Co−O bond lengths of 2.09 Å for Co^{2+} high-spin, identical to that seen in the reported cluster and 1.91 Å for low-spin Co^{3+}, 0.008 Å from the value reported in the structure, whereas for high-spin Co^{3+} the length is 2.00 Å.[16]

However, assumptions based on harmonic frequencies estimated from spectra and bond distances to estimate the reorganization energies were used to argue that the slow ET rate of the cluster is due to anion effects[10]. Notably, the anomaly of the cluster is very similar in magnitude to the anomaly discussed above. An anion is unlikely to have a 10^5−10^6 effect on the rate constant because the outersphere ET is dominated by the structural reorganization associated with changing e_g orbital occupation during redox reaction and not secondary electrostatic effects (**Figures 2-4** where the second-shell hydration effects have modest effect on the trends). Indeed, experimental data for anion effects (sulfates, fluoride, perchlorate *e.g.*) show contributions of only up to five-fold on the rates[12], *i.e.* the anion effect is real but has a magnitude similar to the experimental uncertainty and thus does not contribute much to the five orders of magnitude variation in absolute rates. Notice that a similar magnitude was obtained for the cluster[10]. A much simpler explanation that is quantitatively consistent with all data is that slow ET arises from the large reorganization energy of low-spin Co^{3+}/Co^{2+} due to e_g occupation. The argument that the cluster should induce high-spin to a larger extend than water is not valid because the cluster ligand field is very distinct from hydrated metal ions and the effects of the bridging

ligands on the ligand field strength are not trivial, and additionally comes the effect of water deprotonation not seen in the cluster.

Thus the available data from both NMR, electronic absorption, and cluster exchange studies by Ullman and Nocera are all explainable by very simple electronic structure effects related to orbital occupation, and the involvement of the high-spin state in Co^{3+}(aq).

Conclusions.

The hexaquacobalt(III) complex is not only a much faster electron transfer agent than expected from Marcus cross-relations, it is also a substantially more labile than one would expect from its t_{2g}^6 configuration and +3 charge[17]. Winkler, Rice and Gray discussed this anomaly as possibly due to the involvement of the high-spin state, and estimated it from relaxation of spectroscopic energy terms to be ~17 kJ/mol above the low-spin state[14]. NMR studies in strong acid solution have argued that the high-spin state is >23 kJ/mol above low-spin[18]. Magnetic susceptibility studies by Taube *et al*. arguing for low-spin Co^{3+}(aq) were also carried out in strong acid[17]. Using these three reports, most researchers and text books have settled on the notion that Co^{3+}(aq) is low-spin. The Co^{3+}(aq) system is heterogeneous (including *e.g.* dimer species) and not very stable, preventing study at standard conditions.

In this work we used DFT computations to understand the physics of the relative self-exchange rates. We obtain very consistent results for various functionals, water- and anion models. All data are explained well by simple e_g occupation effects during redox reaction, as evidenced in **Figure 2**. Because these correlate so well with experimental relative rates, they explain most of the ET process. The probability that these linear trends are coincidental is very

small, and it is robust against chemical model and density functional method. Accordingly, most of the electronic reorganization affecting the otherwise similar aqua ions occur in the first hydration sphere *viz*. comparison to a second hydration shell.

The reason why Marcus theory has been claimed to fail can thus be traced to a use of cross relations that involve low-spin Co^{3+} for other systems, whereas we show that involvement of transient high-spin Co^{3+}(aq) produces close to perfect trending with the other data (**Figure 4**). We conclude that Marcus theory remains valid if one uses cross relationships only for the same types of orbital-occupied systems.

Specifically, we conclude that: i) The ~10^5 cobalt anomaly is directly obtained by using low-spin Co^{3+} in a linear regression against other metal ions.; ii) The anomaly is removed to 90% (within the experimental uncertainty) when using instead high-spin Co^{3+} for the deprotonated species, and to essentially 100% when modeling the strong acid system with perchlorate anions (**Figure 5**); these two species control the acid-dependent and –independent processes, respectively. iii) The acid-dependent reorganization energy of $[Co(H_2O)(OH)]^{2+}$ is larger than the acid-independent reorganization energy, explaining the larger rate constant of the acid-independent process[12]. Thus, even if high-spin represents a minor fraction in solution, we conclude that it completely explains the experimental data. The complexity and instability of aqueous Co^{3+} solutions have so far made these insights difficult in the lab, but should be possible to confirm in the future by studying Co^{3+}(aq) mimicking solution and solid-state systems. iv) High-spin Co^{3+}(aq) also explains the standard redox half potential better (Supporting Information, **Figure S2**); v) the trends in experimental data are well described simply by e_g orbital occupation effects because the first coordination sphere dominates the chemistry of these species; vi) As a side consequence, the mechanism of some cobalt-based redox systems that involve processes where similar effects on e_g occupation occur[10] may have to be revisited.

It would, in retrospect, be unusual if the Co^{3+}/Co^{2+} exchange should behave by a distinct mechanism, considering that its activation entropy is similar within 5 kJ/mol of that of the other high-spin $M^{3+/2+(}$aq) outer-sphere processes[11] and considering the overall similarity of these metal ions in aqueous solution. It would also, in retrospect, be unusual that Co^{3+}(aq) shows anomalies both in half standard redox potential, water ligand substitution lability (being more labile than expected for a low-spin Co^{3+} complex), and self-exchange ET that would require three distinct explanations, when, as we show here, high-spin explains them all: The much higher lability than expected of Co^{3+}(aq) during ligand substitution in water directly follows from high-spin having substantially longer and weaker Co-O bonds (see Supporting Information, **Tables S44-S57**); these various well-known anomalies are consistent with our results and interpretations. As a final remark, also in retrospect, there is indeed previous evidence for 6-O Co(III) complexes having high-spin involvement, notably those produced by Kläui and co-workers[58,59] and very recently by Cummins and co-workers[60].

Acknowledgements. Computer time at the Steno cluster at DTU Chemistry is gratefully acknowledged.

Supporting Information available. The supporting information contains a pdf file with electronic energies, calculated corrections, sensitivity tests that use different experimental data, and linear regression data, and a separate file with all the optimized structures as xyz coordinates.

References.

(1) Libby, W. F. Theory of Electron Exchange Reactions in Aqueous Solution. *J. Phys. Chem.* **1952**, *56* (7), 863–868.

(2) Marcus, R. A.; Sutin, N. Electron Transfers in Chemistry and Biology. *Biochim. Biophys. Acta - Reviews Bioenerg.* **1985**, *811* (3), 265–322.

(3) Blumberger, J. Recent Advances in the Theory and Molecular Simulation of Biological Electron Transfer Reactions. *Chem. Rev.* **2015**, *115* (20), 11191–11238.

(4) Beinert, H.; Holm, R. H.; Münck, E. Iron-Sulfur Clusters: Nature's Modular, Multipurpose Structures. *Science* **1997**, *277* (5326), 653–659.

(5) Hush, N. S. Adiabatic Theory of Outer Sphere Electron-Transfer Reactions in Solution. *Trans. Faraday Soc.* **1961**, *57*, 557–580.

(6) Kuznetsov, A. M.; Ulstrup, J. *Electron Transfer in Chemistry and Biology: An Introduction to the Theory*; John Wiley & Sons Ltd, 1999.

(7) Hush, N. S. Distance Dependence of Electron Transfer Rates. *Coord. Chem. Rev.* **1985**, *64*, 135–157.

(8) Marcus, R. A. On the Theory of Oxidation□Reduction Reactions Involving Electron Transfer. I. *J. Chem. Phys.* **1956**, *24* (5).

(9) Newton, M. D.; Sutin, N. Electron Transfer Reactions in Condensed Phases. *Annu. Rev. Phys. Chem.* **1984**, *35* (1), 437–480.

(10) Ullman, A. M.; Nocera, D. G. Mechanism of Cobalt Self-Exchange Electron Transfer. *J. Am. Chem. Soc.* **2013**, *135* (40), 15053–15061.

(11) Weaver, M. J.; Yee, E. L. Activation Parameters for Homogeneous Outer-Sphere Electron-Transfer Reactions. Comparisons between Self-Exchange and Cross Reactions Using Marcus' Theory. *Inorg. Chem.* **1980**, *19* (7), 1936–1945.

(12) Habib, H. S.; Hunt, J. P. Electron-Transfer Reactions between Aqueous Cobaltous and Cobaltic Ions. *J. Am. Chem. Soc.* **1966**, *88* (8), 1668–1671.

(13) Endicott, J. F.; Durham, B.; Kumar, K. Examination of the Intrinsic Barrier to Electron Transfer in hexaaquacobalt(III): Evidence for Very Slow Outer-Sphere Self-Exchange Resulting from Contributions of Franck-Condon and Electronic Terms. *Inorg. Chem.* **1982**, *21* (6), 2437–2444.

(14) Winkler, J. R.; Rice, S. F.; Gray, H. B. On the Role of the High-Spin State in the Water Exchange Reaction of Hexaaquocobalt(III). *Comments Inorg. Chem.* **1981**, *1* (1), 47–51.

(15) Macartney, D. H.; Sutin, N. Kinetics of the Oxidation of Metal Complexes by manganese(III) Aquo Ions in Acidic Perchlorate Media: The $Mn(H_2O)_6^{2+}$-$Mn(H_2O)_6^{3+}$ Electron-Exchange Rate Constant. *Inorg. Chem.* **1985**, *24* (21), 3403–3409.

(16) Mortensen, S. R.; Kepp, K. P. Spin Propensities of Octahedral Complexes From Density Functional Theory. *J. Phys. Chem. A* **2015**, *119*, 4041–4050.

(17) Friedman, H. L.; Hunt, J. P.; Plane, R. A.; Taube, H. The Magnetic Susceptibility of Co+++aq. *J. Am. Chem. Soc.* **1951**, *73* (8), 4028–4030.

(18) Navon, G. A Search for the Thermally Populated High-Spin Excited State of hexaaquocobalt(3+) by Coblt NMR. *J. Phys. Chem.* **1981**, *85* (24), 3547–3549.

(19) Johnson, D. A.; Sharpe, A. G. Reactions of cobalt(III) Compounds: Magnitude of Cobalt(III)/Cobalt(II) Standard Potential in Aqueous Solution. *J. Chem. Soc.* **1964**, 3490–3492.

(20) Wangila, G.; Jordan, R. B. A Convenient Source of hexaaquacobalt(III). *Inorganica Chim. Acta* **2003**, *343* (Supplement C), 347–350.

(21) Johnson, D. A.; Sharpe, A. G.; Morss, L. R.; Jolly, W. L. Cesium Cobalt(III) Sulfate 12-Hydrate. In *Inorganic Syntheses*; John Wiley & Sons, Inc., 1967; pp 61–63.

(22) Johnson, D. A.; Nelson, P. G. Thermodynamic Properties of Co^{3+}(Aq). *J. Chem. Soc. Dalt. Trans.* **1990**, No. 1, 1–4.

(23) Kepp, K. P. Consistent Descriptions of Metal–ligand Bonds and Spin-Crossover in Inorganic Chemistry. *Coord. Chem. Rev.* **2013**, *257* (1), 196–209.

(24) Kepp, K. P. Theoretical Study of Spin Crossover in 30 Iron Complexes. *Inorg. Chem.* **2016**, *55* (6), 2717–2727.

(25) Gütlich, P.; Goodwin, H. A. Spin Crossover—an Overall Perspective. In *Spin Crossover in Transition Metal Compounds I*; Springer, 2004; pp 1–47.

(26) Sisley, M. J.; Jordan, R. B. First Hydrolysis Constants of Hexaaquacobalt (III) and-Manganese (III): Longstanding Issues Resolved. *Inorg. Chem.* **2006**, *45* (26), 10758–10763.

(27) Tretter, L.; Adam-Vizi, V. Inhibition of Krebs Cycle Enzymes by Hydrogen Peroxide: A Key Role of [Alpha]-Ketoglutarate Dehydrogenase in Limiting NADH Production under Oxidative Stress. *J. Neurosci.* **2000**, *20* (24), 8972–8979.

(28) Chou, M.; Creutz, C.; Sutin, N. Rate Constants and Activation Parameters for Outer-

Sphere Electron-Transfer Reactions and Comparisons with the Predictions of Marcus Theory. *J. Am. Chem. Soc.* **1977**, *99* (17), 5615–5623.

(29) Brunschwig, B. S.; Creutz, C.; Macartney, D. H.; Sham, T. K.; Sutin, N. The Role of Inner-Sphere Configuration Changes in Electron-Exchange Reactions of Metal Complexes. *Faraday Discuss. Chem. Soc.* **1982**, *74*, 113–127.

(30) Bonner, N. A.; Hunt, J. P. The Exchange Reaction between Cobaltous and Cobaltic Ions in Perchloric Acid Solution. *J. Am. Chem. Soc.* **1952**, *74* (7), 1866.

(31) Anderson, A.; Bonner, N. A. The Exchange Reaction between Chromous and Chromic Ions in Perchloric Acid Solution. *J. Am. Chem. Soc.* **1954**, *76* (14), 3826–3830.

(32) Ahlrichs, R.; Bär, M.; Häser, M.; Horn, H.; Kölmel, C. Electronic Structure Calculations on Workstation Computers: The Program System Turbomole. *Chem. Phys. Lett.* **1989**, *162* (3), 165–169.

(33) Eichkorn, K.; Treutler, O.; Öhm, H.; Häser, M.; Ahlrichs, R. Auxiliary Basis Sets to Approximate Coulomb Potentials. *Chem. Phys. Lett.* **1995**, *240* (4), 283–290.

(34) Weigend, F.; Häser, M. RI-MP2: First Derivatives and Global Consistency. *Theor. Chem. Acc.* **1997**, *97* (1), 331–340.

(35) Weigend, F.; Ahlrichs, R. Balanced Basis Sets of Split Valence, Triple Zeta Valence and Quadruple Zeta Valence Quality for H to Rn: Design and Assessment of Accuracy. *Phys. Chem. Chem. Phys.* **2005**, *7* (18), 3297–3305.

(36) Perdew, J. P.; Burke, K.; Ernzerhof, M. Generalized Gradient Approximation Made Simple. *Phys. Rev. Lett.* **1996**, *77* (18), 3865.

(37) Becke, A. D. Density□functional Thermochemistry. III. The Role of Exact Exchange. *J.*

Chem. Phys. **1993**, *98* (7), 5648–5652.

(38) Stephens, P. J.; Devlin, F. J.; Chabalowski, C. F.; Frisch, M. J. Ab Initio Calculation of Vibrational Absorption and Circular Dichroism Spectra Using Density Functional Force Fields. *J. Phys. Chem.* **1994**, *98* (45), 11623–11627.

(39) Lee, C.; Yang, W.; Parr, R. G. Development of the Colle-Salvetti Correlation-Energy Formula into a Functional of the Electron Density. *Phys. Rev. B* **1988**, *37* (2), 785–789.

(40) Tao, J.; Perdew, J. P.; Staroverov, V. N.; Scuseria, G. E. Climbing the Density Functional Ladder: Nonempirical Meta Generalized Gradient Approximation Designed for Molecules and Solids. *Phys. Rev. Lett.* **2003**, *91* (14), 146401.

(41) Perdew, J. P.; Tao, J.; Staroverov, V. N.; Scuseria, G. E. Meta-Generalized Gradient Approximation: Explanation of a Realistic Nonempirical Density Functional. *J. Chem. Phys.* **2004**, *120* (15).

(42) Nelsen, S. F.; Blackstock, S. C.; Kim, Y. Estimation of Inner Shell Marcus Terms for Amino Nitrogen Compounds by Molecular Orbital Calculations. *J. Am. Chem. Soc.* **1987**, *109* (3), 677–682.

(43) Klamt, A.; Schüürmann, G. COSMO: A New Approach to Dielectric Screening in Solvents with Explicit Expressions for the Screening Energy and Its Gradient. *J. Chem. Soc. Perkin Trans. 2* **1993**, No. 5, 799–805.

(44) Schäfer, A.; Klamt, A.; Sattel, D.; Lohrenz, J. C. W.; Eckert, F. COSMO Implementation in TURBOMOLE: Extension of an Efficient Quantum Chemical Code towards Liquid Systems. *Phys. Chem. Chem. Phys.* **2000**, *2* (10), 2187–2193.

(45) Jensen, K. P. Iron–sulfur Clusters: Why Iron? *J. Inorg. Biochem.* **2006**, *100*, 1436–1439.

(46) Kepp, K. P. Halide Binding and Inhibition of Laccase Copper Clusters: The Role of Reorganization Energy. *Inorg. Chem.* **2014**, *54* (2), 476–483.

(47) Jensen, K. P.; Ooi, B.-L.; Christensen, H. E. M. Accurate Computation of Reduction Potentials of 4Fe-4S Clusters Indicates a Carboxylate Shift in Pyrococcus Furiosus Ferredoxin. *Inorg. Chem.* **2007**, *46* (21), 8710–8716.

(48) Jensen, K. P. Computational Studies of Modified $[Fe_3S_4]$ Clusters: Why Iron Is Optimal. *J. Inorg. Biochem.* **2008**, *102*, 87–100.

(49) Jensen, K. P.; Rykær, M. The Building Blocks of Metallothioneins: Heterometallic Zn^{2+} and Cd^{2+} Clusters from First-Principles Calculations. *Dalt. Trans.* **2010**, *39*, 9684.

(50) Grimme, S.; Antony, J.; Ehrlich, S.; Krieg, H. A Consistent and Accurate Ab Initio Parametrization of Density Functional Dispersion Correction (DFT-D) for the 94 Elements H-Pu. *J. Chem. Phys.* **2010**, *132* (15), 154104.

(51) Stuenzi, H.; Marty, W. Early Stages of the Hydrolysis of Chromium (III) in Aqueous Solution. 1. Characterization of a Tetrameric Species. *Inorg. Chem.* **1983**, *22* (15), 2145–2150.

(52) Meier, R.; Boddin, M.; Mitzenheim, S.; Kanamori, K. Solution Properties of Vanadium (III) with Regard to Biological Systems. *Met. Ions Biol. Syst.* **1995**, *31*, 45.

(53) Delahay, P.; Dziedzic, A. Inner□sphere Reorganization in Optical Electron Transfer. *J. Chem. Phys.* **1984**, *80* (11), 5793–5798.

(54) Jensen, K. P.; Cirera, J. Accurate Computed Enthalpies of Spin Crossover in Iron and Cobalt Complexes. *J. Phys. Chem. A* **2009**, *113*, 10033–10039.

(55) Elliot, A. J.; McCracken, D. R.; Buxton, G. V; Wood, N. D. Estimation of Rate Constants

for near-Diffusion-Controlled Reactions in Water at High Temperatures. *J. Chem. Soc. Faraday Trans.* **1990**, *86* (9), 1539–1547.

(56) Sutin, N. Nuclear, Electronic, and Frequency Factors in Electron Transfer Reactions. *Acc. Chem. Res.* **1982**, *15* (9), 275–282.

(57) Jensen, K. P.; Roos, B. O.; Ryde, U. Performance of Density Functionals for First Row Transition Metal Systems. *J. Chem. Phys.* **2007**, *126*, 14103.

(58) Gütlich, P.; McGarvey, B. R.; Kläui, W. Temperature-Dependent $^5T_2$ (O_h) ⇌ $^1A_1$ (O_h) Spin Equilibrium in a Six-Coordinate Cobalt (III) Complex. Investigation by Phosphorus-31 NMR in Solution. *Inorg. Chem.* **1980**, *19* (12), 3704–3706.

(59) Kläui, W. High Spin-Low Spin Equilibrium in Six-Coordinate cobalt(III) Complexes. *Inorganica Chim. Acta* **1980**, *40* (40).

(60) Stauber, J. M.; Zhang, S.; Gvozdik, N.; Jiang, Y.; Avena, L.; Stevenson, K. J.; Cummins, C. C. Cobalt and Vanadium Trimetaphosphate Polyanions: Synthesis, Characterization, and Electrochemical Evaluation for Non-Aqueous Redox-Flow Battery Applications. *J. Am. Chem. Soc.* **2018**, *140* (2), 538–541.

Table of Content Graphic.

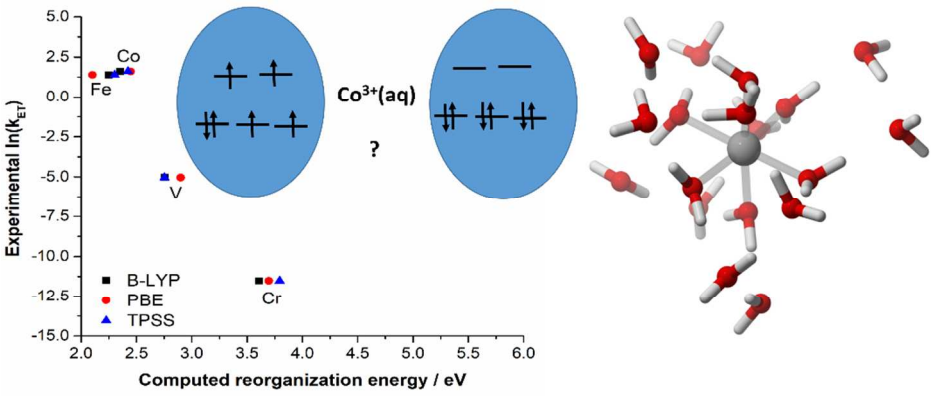

Synopsis.

We studied the classic self-exchange ET processes of hydrated transition metal ions. We identify directly the ~10^5 anomaly of Co^{2+}/Co^{3+}(aq) from the electronic reorganization energies. We show that with high-spin Co^{3+}, the anomaly disappears, and that the high-spin state is more important than previously thought after correcting experimental data by DFT-derived data. We conclude that high-spin Co^{3+}(aq) is chemically active and that Co^{3+}(aq) is close to spin crossover.

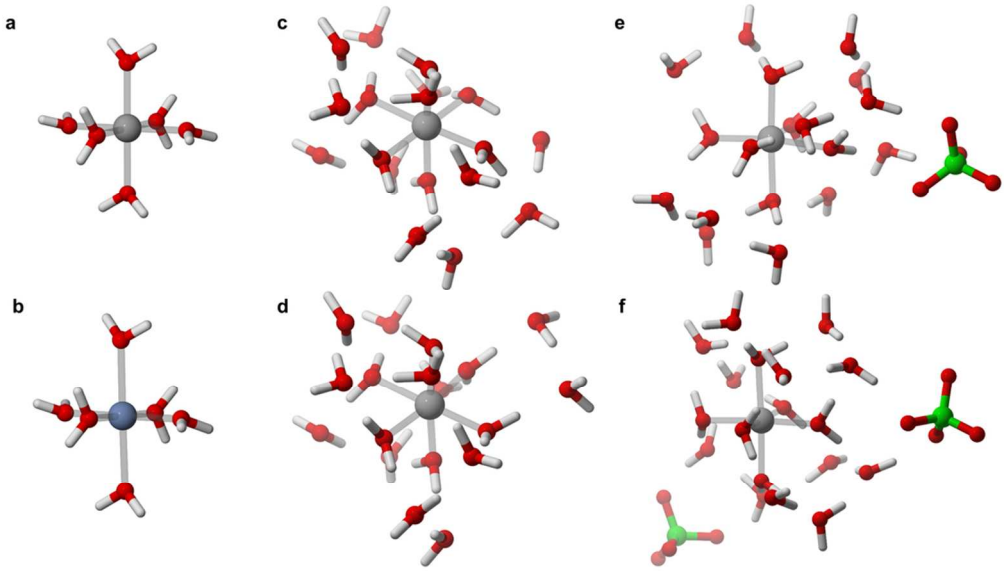

Figure 1

95x55mm (300 x 300 DPI)

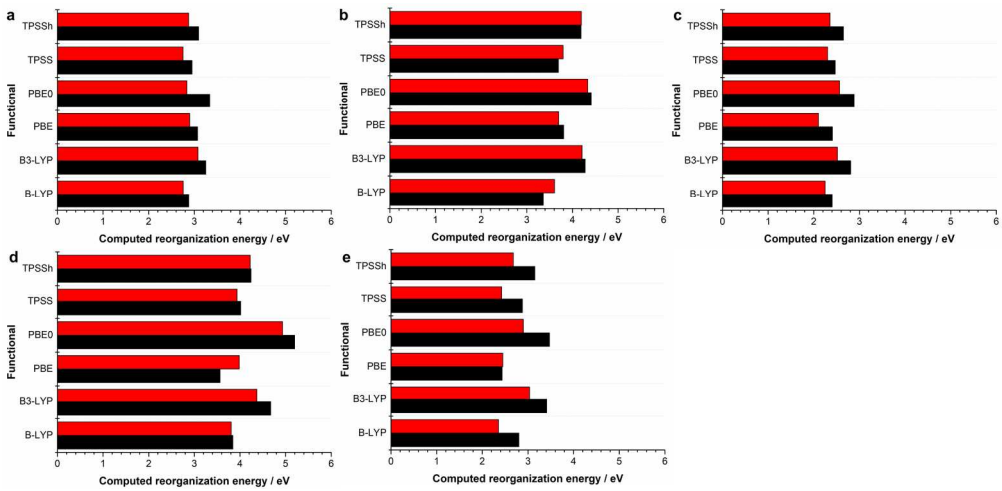

Figure 2

175x85mm (300 x 300 DPI)

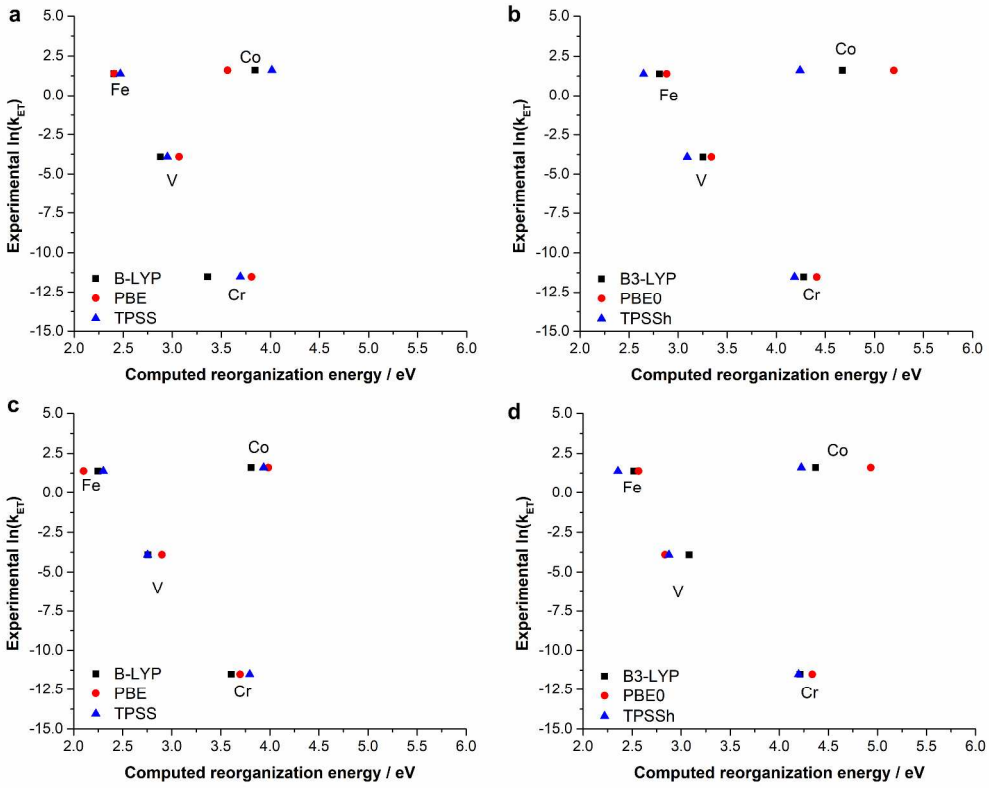

Figure 3

474x374mm (300 x 300 DPI)

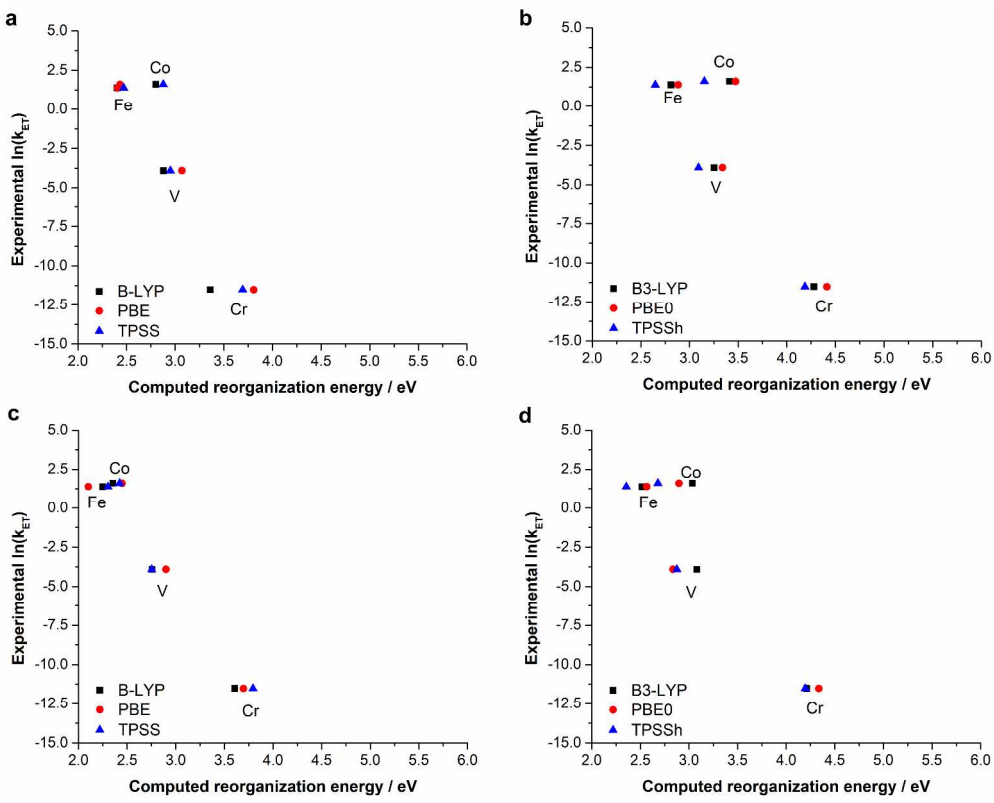

Figure 4

478x381mm (300 x 300 DPI)

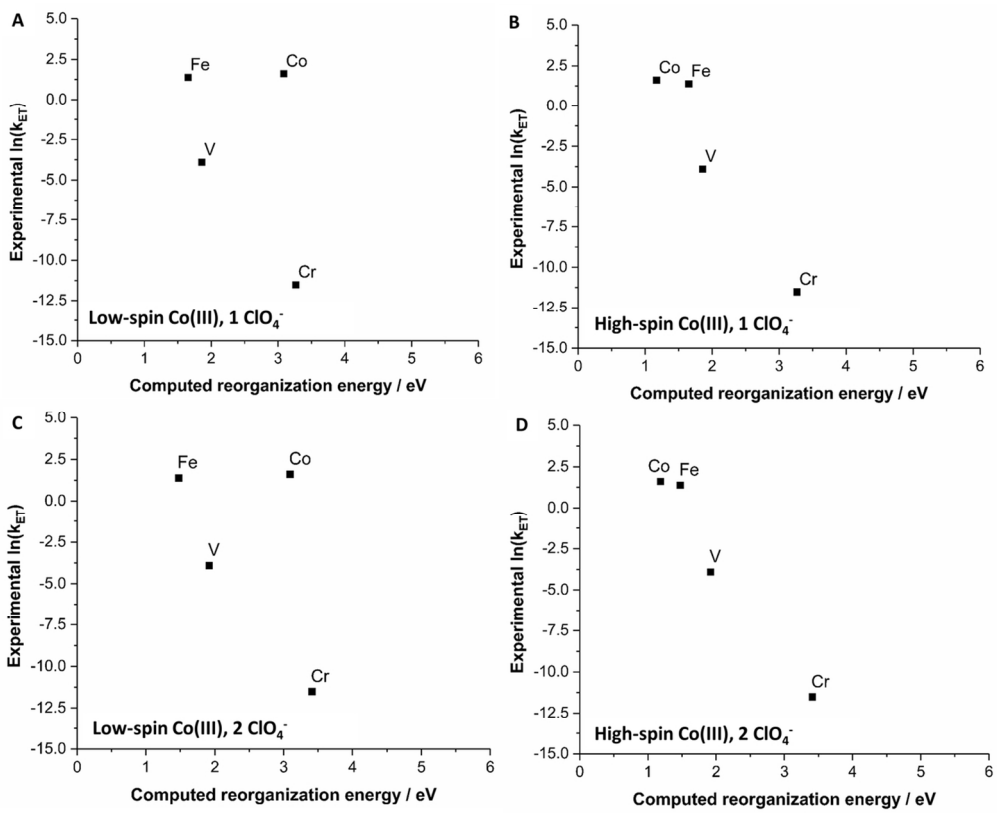

Figure 5

113x92mm (300 x 300 DPI)

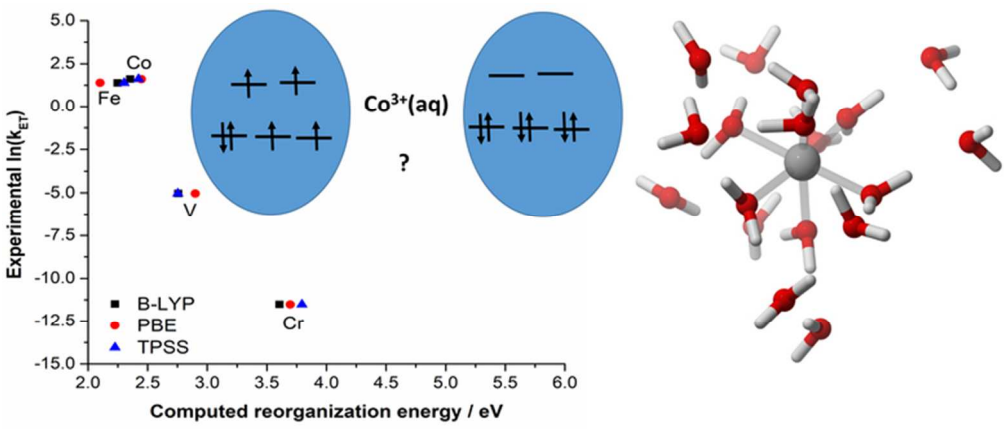

TOC graphic

65x27mm (300 x 300 DPI)